Large-Area Single-Layer $MoSe_2$ and Its van der Waals Heterostructures

Gi Woong Shim,[†,§] Kwonjae Yoo,[‡,§] Seung-Bum Seo,[†] Jongwoo Shin,[†] Dae Yool Jung,[†] Il-Suk Kang,[‡] Chi Won Ahn,[‡] Byung Jin Cho,[†] and Sung-Yool Choi[†,*]

[†]Department of Electrical Engineering and Graphene Research Center, Korea Advanced Institute of Science and Technology (KAIST), Daejeon 305-701, Republic of Korea, and [‡]National Nanofab Center, Korea Advanced Institute of Science and Technology (KAIST), Daejeon 305-806, Republic of Korea. [§]G. W. Shim and K. Yoo contributed equally to this work.

ABSTRACT Layered structures of transition metal dichalcogenides stacked by van der Waals interactions are now attracting the attention of many researchers because they have fascinating electronic, optical, thermoelectric, and catalytic properties emerging at the monolayer limit. However, the commonly used methods for preparing monolayers have limitations of low yield and poor extendibility into large-area applications. Herein, we demonstrate the synthesis of large-area $MoSe_2$ with high quality and uniformity by selenization of MoO_3 *via* chemical vapor deposition on arbitrary substrates such as SiO_2 and sapphire. The resultant monolayer was intrinsically doped, as evidenced by the formation of charged excitons under low-temperature photoluminescence analysis. A van der Waals heterostructure of $MoSe_2$ on graphene was also demonstrated. Interestingly, the $MoSe_2$/graphene heterostructures show strong quenching of the characteristic photoluminescence from $MoSe_2$, indicating the rapid transfer of photogenerated charge carriers between $MoSe_2$ and graphene. The development of highly controlled heterostructures of two-dimensional materials will further promote advances in the physics and chemistry of reduced dimensional systems and will provide novel applications in electronics and optoelectronics.

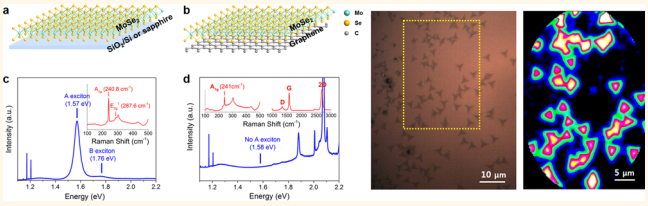

KEYWORDS: $MoSe_2$ · monolayer · chemical vapor deposition · van der Waals heterostructure

The separation of a single layer of hexagonally arranged carbon atoms from van der Waals stacked bulk graphite opened a new era in nanotechnology based on the novel perspectives it provided in many fields of research. The peculiar properties emanating from the monolayer limit make graphene a most suitable ingredient for future integrative technology. However, regardless of the outstanding nature of graphene, its semimetallic properties, coming from its zero band gap,[1] make it hard to replace conventional Si-based technology. Therefore, two-dimensional (2D) materials having a band gap lying in between the semiconducting regime[2−4] have emerged to complement the shortcomings of graphene. The representative materials of those classes are transition metal dichalcogenides (TMDCs) such as MoS_2, $MoSe_2$, WS_2, and WSe_2.

Since the first isolation of single-layer MoS_2 was reported in 2010,[5] researchers have found many interesting properties including its enhanced optical absorption,[6,7] unusually high photocurrent generation driven by photothermal effect,[8] efficient hydrogen evolution reaction capability,[9] valley polarization,[10] and high on/off ratio with low subthreshold swing,[11] which can lead to ultrathin and highly efficient photovoltaics, photothermoelectrics, catalysis for sustainability, valleytronics, and low-power electronics. However, the problem is that the previous approaches used for material manufacturing have been mostly based on mechanical[2−8] and chemical exfoliation,[9,12−14] which have limitations in size, reproducibility, and low throughput. Therefore, synthetic approaches based on chemical vapor deposition (CVD) are required for preparing 2D materials in large area with uniformity, to demonstrate those appealing properties practically. The synthesis of MoS_2, WS_2, and WSe_2 monolayers by CVD was reported in 2012 and 2013.[15−18] However, the preparation of $MoSe_2$ monolayers in large area has still been a great challenge.

In this study, we report the synthesis of $MoSe_2$ monolayers in large area. Thermal

* Address correspondence to sungyool.choi@kaist.ac.kr.

Received for review November 1, 2013 and accepted July 2, 2014.

Published online July 02, 2014
10.1021/nn405685j

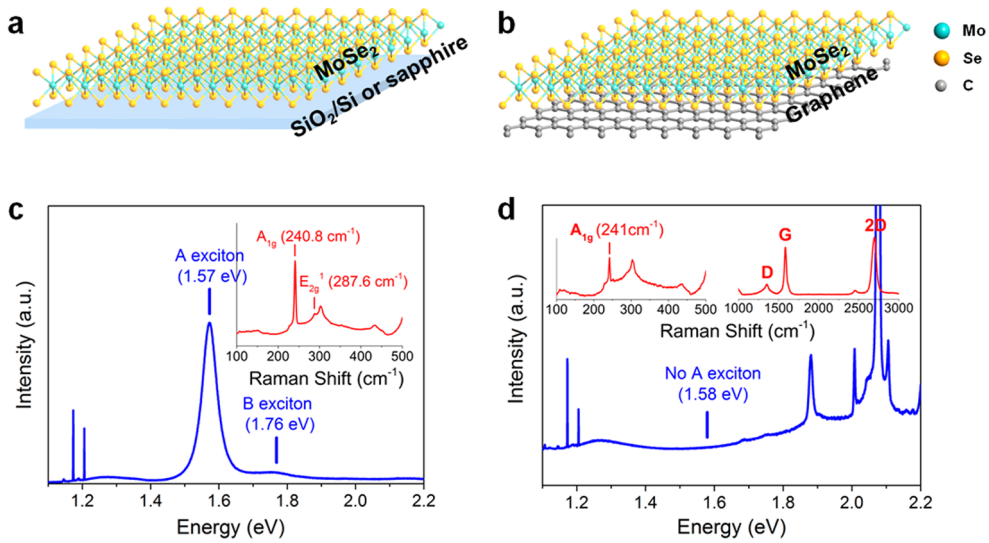

Figure 1. Single-layer $MoSe_2$ grown on various substrates by CVD. (a, b) Schematic of monolayer $MoSe_2$ on SiO_2/Si or sapphire substrate, and graphene. (c, d) PL spectra of the as-synthesized $MoSe_2$ monolayer films on SiO_2/Si and graphene/SiO_2/Si. Raman data from the same samples are shown in the inset.

chemical vapor deposition, based on reactions between Se and MoO_3 at low pressure, resulted in the limited growth of $MoSe_2$ monolayers in large area, estimated as 1.5 cm × 2 cm, with extremely high uniformity. Also, the process is applicable on various substrates such as SiO_2 and sapphire, which reduces current problems in transfer processes, including monolayer folding, covering with nonuniformity, and chemical degradability of monolayers. The observation of monotonically decreased intensities of excitonic photoluminescence (PL) with temperature confirmed monolayers with direct band gap.[4] Also, the emergence of red-shifted peaks at 27 meV lower than excitonic peaks in the low-temperature regime indicated intrinsic doping in the monolayered film on the substrate.[22,23] Meanwhile, unusual behaviors of excited charge carriers in van der Waals epitaxial $MoSe_2$/graphene heterostructures were investigated and were explained by readily transferred charge carriers to graphene followed by nonradiative decay. We believe the newly generated band energy levels of this $MoSe_2$ monolayer complement previously synthesized 2D materials and can provide more diverse combinations of materials for photovoltaics, potential barriers in catalysis, and electron/hole transport systems. Also, investigating the mechanism of charge transfer in the $MoSe_2$/graphene interface can help fully resolve existing problems in photovoltaics and optoelectronics.

RESULTS AND DISCUSSION

Synthesis of a $MoSe_2$ monolayer was achieved by using insulating substrates (SiO_2/Si and sapphire) and graphene as a template, and the final structures of the as-synthesized $MoSe_2$ are described in Figure 1. Here, the Mo atoms are sandwiched in between Se with trigonal prismatic coordinations. Considering the in-plane lattice parameters of the $MoSe_2$ monolayer (0.331 nm),[19] (0001)-oriented sapphire substrate (0.476 nm),[20] and graphene (0.248 nm),[7] the lattice mismatch is estimated to be 30% for $MoSe_2$/sapphire and 33% for $MoSe_2$/graphene structures. Even though significant strains are applied at the interfaces, the templated growth using graphene resulted in epitaxially grown $MoSe_2$ over a large area with novel optical properties. The structural and optical analyses of the heterostructures are depicted in Figures S2 and 1d.

The identification of each of the structures was mostly done by optical characterization tools, with Raman shift and PL energy. It is well known that the out-of-plane A_{1g} vibration mode of single-layer $MoSe_2$ appears at a Raman shift of 241 cm^{-1}[21] (also, the peak position of our reference data collected from the mechanically exfoliated monolayer $MoSe_2$ exactly matches those of CVD-grown samples; refer to Figure S3) and the bilayer at 242 cm^{-1}. The in-plane E_{2g}^1 mode shows up at 287 cm^{-1} for monolayer and 286 cm^{-1} for bilayer samples[21] (also refer to Figure S3), although the reported values have slight variations depending on the experimental setup and calibrations. About 1 cm^{-1} of differences in Raman shift originate from lattice stiffening induced by van der Waals interactions between layers,[21] which is a very strong and reliable tool to optically differentiate mono-, bi-, and multilayered samples. Considering that the energy differences in the E_{2g}^1 and A_{1g} vibration modes become smaller with the number of layers (*i.e.*, blue-shifts for A_{1g} and red-shifts for E_{2g}^1), our Raman data in Figure 1c clearly confirm that the as-deposited film is a single layer. The out-of-plane vibration mode of B_{2g}^1 at 353 cm^{-1} is forbidden and has almost neglibile intensity for monolayers but has similar or higher

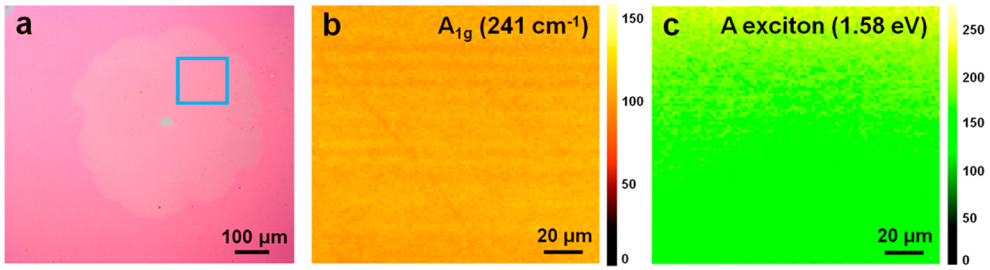

Figure 2. (a) Optical image of the as-grown $MoSe_2$ monolayer on SiO_2/Si substrate. (b, c) The marked region in (a) was intensity mapped by using (a) the A_{1g} vibration mode in Raman (234−246 cm^{-1}) and (c) direct A excitonic transition peak in PL (1.43−1.7 eV) as references. The standard deviation over the average intensity was calculated as 0.033 for (b) and 0.147 for (c), and an Ar-ion laser with 514.5 nm wavelength excitation source was used for all characterizations.

intensity for bilayer samples compared with the $E_{2g}{}^1$ mode[21] (also refer to Figure S3). Here, we could not observe any trace of $E_{2g}{}^1$ mode at around 353 cm^{-1}, which also proves the authenticity of our monolayer sample.

In addition to Raman spectroscopy, PL analysis is another powerful tool for characterizing the atomically thin layers of TMDCs. Generally, three peaks appear in PL spectra: one is from indirect (Γ-to-K) band transition and the other two are from direct (K-to-K) transition. The indirect band gap is a commonly observed feature in a bulk material, while the direct band gap appears only with monolayer samples. It is generally believed that strong quantum confinement in the direction perpendicular to the surface renders the band gap direct when the thickness of $MoSe_2$ goes to the atomic limit.[5] Interestingly, the extraordinary behavior of significantly large peak separations of 0.1−0.4 eV in direct band transition peaks has been observed in monolayer TMDCs, as affected by giant spin−orbit coupling from heavy atoms with large angular momentum.[21−23] The resultant valence band splitting was reflected in PL spectra. The transition from the upper valence band corresponds to A excitonic and the lower to B excitonic transition. The presence of a B excitonic energy level plays a significant role in valleytronics, so its elucidation is of great importance. However, as far as we know, the B excitonic transition of a $MoSe_2$ monolayer in PL has not been reported yet. Though the formation of a B exciton has been demonstrated by differential reflectance spectra,[22] that study did not provide any useful information about the preference for each transition. The negligible intensity of B excitonic peaks compared with A excitonic peaks[24] is attributed to difficulties in identifications of B excitonic transitions.

Here, we discovered both the A excitonic peak at 1.58 eV and the B excitonic peak at 1.76 eV. The ratio of the peak intensities is estimated to be I_A/I_B = 10−15, and the valence band splitting of 0.18−0.19 eV is in excellent agreement with the experimental and the theoretical data in previous reports.[19,22−24]

Also, a most intriguing phenomenon occurring at the interface of graphene/$MoSe_2$ was revealed, as represented by significant reduction in the PL intensity of $MoSe_2$ while its intensities were conserved in the Raman spectrum. The detailed mechanisms will be further discussed in a later part of the paper.

An optical image of the as-grown $MoSe_2$ monolayer on SiO_2/Si is indicated in Figure 2a. The shape resembles a circle, which deviates from the theoretically predicted forms (triangular) at the thermodynamic equilibrium,[15,16] implying that the kinetics (probably favor undefined edges and irregular shapes[18,26]) would take part in determining the final shape together with thermodynamics. For example, the growth occurred at low reducing environment and resulted in distorted triangular forms with bow-type edges as affected by kinetics, while almost triangular mono- to few-layered samples were attained at highly reducing conditions with H_2 flow as the reduction in reaction barrier by H_2 brought thermodynamics more dominant.[25] Similarly, the separate experiment here with the same apparatus but at relatively low temperature and reducing environment gave triangular and star-shaped monolayer $MoSe_2$, as indicated in Figures S9 and S10. Therefore, the formation of circularly shaped $MoSe_2$ on Figure 2a is thought to be driven by kinetic factors, which are represented by significant interactions between the atomically very thin $MoSe_2$ and the substrate, the amorphous nature of the surfaces, and low reducing atmosphere. When using graphene as templates, the alignment of all the carbon atoms facilitates the van der Waals interactions between the substrate and growing $MoSe_2$ and results in epitaxial growth and more distinguishable, sharp edges and vertexes. Growth driven by the directed weak interactions was further confirmed by scanning transmission electron microscopy (STEM), and those results are presented in Figure S2.

In any case, whichever shape is attained, the conventional mechanism of nucleation at the center followed by growth in all lateral directions with similar propagation rates is crystal clear, as evident in the optical microscope (OM) images of Figure 2a.

To clarify that the as-grown $MoSe_2$ monolayer was uniform over large area, Raman and PL mapping were performed. The rectangular region in Figure 2a was intensity mapped. The A_{1g} (234−246 cm^{-1}) and A

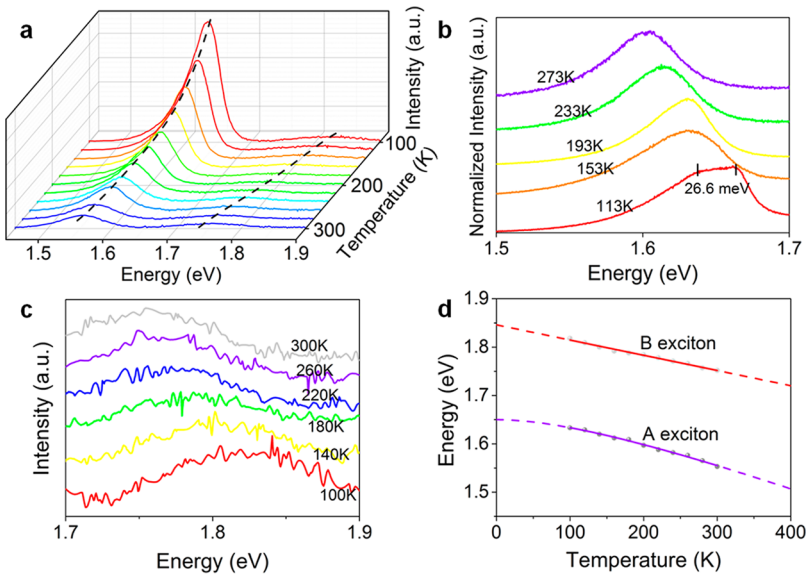

Figure 3. (a) PL spectra of $MoSe_2$ monolayer acquired from 100 to 300 K. (b) Emergence of the trion peaks below 153 K, as elucidated by PL measurements of A excitonic peaks at various temperatures. (c) The 17× magnified profile of B excitonic peaks of (a). (d) Temperature-dependent behavior of A and B excitonic transition energy. Each value was fitted by the empirical Varshni equation.

excitonic transition (1.43−1.7 eV) peaks, which are the most notable peaks in Raman and PL, were set to a reference. In addition to the peak intensities, the peak position also showed the extreme uniformity of the as-synthesized films (see Supporting Information Figure S5). Here, most of the A_{1g} vibration mode lay within the range 240.7−240.9 cm^{-1} and the PL peaks were in the 1.583−1.585 eV range. Taking into account that the bilayer of our exfoliated samples showed A_{1g} peaks at 1 cm^{-1} apart from the A_{1g} of a monolayer (*i.e.*, 242 cm^{-1}), and the A excitonic peak of a bilayer sample appeared at 1.54−1.55 eV, which is red-shifted 0.03 eV from a monolayer, it ultimately confirms a highly uniform $MoSe_2$ monolayer grown over a large area. In Figures S4 and S5, intensity and peak position mapping images of the $MoSe_2$ grown on a sapphire substrate are shown, which also indicate the high quality of our samples on arbitrary substrates.

In addition to the previous measurements of Raman/PL at room temperature, low-temperature PL experiments are alternative ways of determining the number of layers and providing valuable information for understanding intrinsic material properties. The temperature-dependent PL spectra are presented in Figure 3a. The PL intensity of $MoSe_2$ gradually increases with a decrease in temperature, implying an enhanced exciton lifetime at low temperatures. The reduced thermal vibrations of the lattice are thought to drive this process by suppressing nonradiative electron−hole recombination.[4,22] Such temperature-dependent responses in PL intensities are unique features in the monolayer of TMDCs with a direct band gap. For TMDCs with more than two layers, the nature of the indirect band gap results in competitions between decay channels K-to-K (direct) and Γ-to-K (indirect). Since the indirect transition becomes more feasible at high temperatures, while the direct transition is more preferred at low temperatures, the few-layered TMDC shows its local minimum in PL intensity at a certain temperature. Usually the temperature lies below the room temperature.[4,27] Therefore, our measurements of PL at various temperatures could verify the nature of the monolayer sample.

When the temperature increases, a rise in thermal energy renders an expanded lattice, which brings decreased potential confinements and a decrease in energy band gap.[28] The results are well reflected in Figure 3a. Here, both A and B excitonic peaks were red-shifted with temperature. The Varshni equation, an empirical description of temperature-dependent band gap behaviors, is represented by

$$E_g = E_{g0} - \frac{\alpha T^2}{T + \beta} \quad (1)$$

where E_{g0} corresponds to the band gap at 0 K and α and β are fitting parameters.[29] Considering the valence band splitting by spin−orbit coupling, the optical band gap at absolute 0 K is estimated as $(E_{g0,A} + E_{g0,B})/2$ = (1.650 + 1.846)/2 eV = 1.748 eV, which is fairly consistent with the previous reports of theoretical values of 1.72 eV obtained by density functional theory (DFT) based on first-principles using the GGA-PBE functional.[30] Other parameters were $\alpha = 5.82 \times 10^{-4}$ eV/K, $\beta = 251$ K for A excitonic transition and $\alpha = 3.15 \times 10^{-4}$ eV/K, $\beta = 0.277$ K for B excitonic transition.

Understanding the nature of intrinsically doped samples of monolayer TMDCs on a substrate is crucial for fabricating devices and diverse applications. The commonly observed doping type of $MoSe_2$ is n-type,[31]

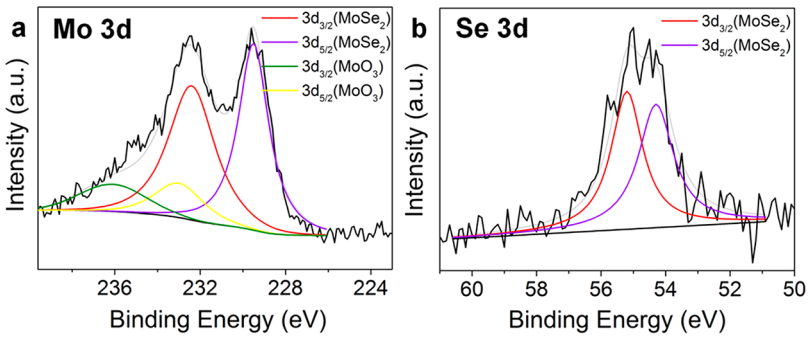

Figure 4. (a, b) XPS spectra of the as-grown $MoSe_2$ monolayer on SiO_2/Si substrate. The binding energy of (a) Mo 3d and (b) Se 3d was resolved for chemical analysis.

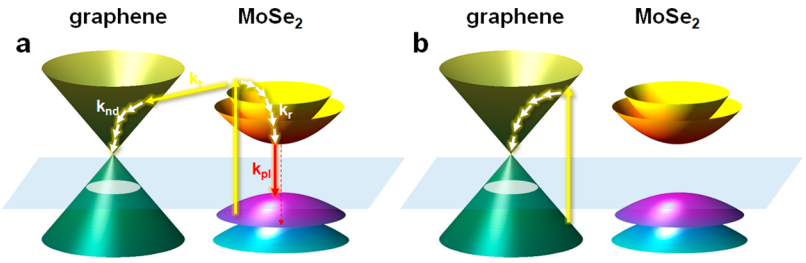

Figure 5. Proposed photogenerated charge transfer mechanisms at the p-doped graphene/$MoSe_2$ interfaces. Transfer processes of the excited charge carriers in (a) $MoSe_2$ and (b) graphene. The energy of irradiated light is presumed to be greater than the A excitonic transition energy of the $MoSe_2$ monolayer (1.58 eV).

and the surface doping effect is understood to originate from a buildup of defects at the surfaces and/or surface interactions.[31,32] Here, the nature of doped samples can be inferred by low-temperature measurements of PL spectra. At a sufficiently low temperature regime, a trion, a kind of charged unit consisting of an electron or a hole added to an exciton, can stably exist. The trion binding energy is usually very small compared with that of an exciton, and the value is comparable to thermal energy at room temperature.[33] Therefore, it easily dissociates into an exciton together with an electron/hole at sufficiently high temperatures. At temperatures below 153 K, the formation of a trion in our sample was evidenced by an additional peak appearing at 27 meV lower than the excitonic peaks. The difference in peak separation matches well with the previously reported theoretical and experimental data.[22,33] Meanwhile, a peak at 1.5−1.6 eV, which originated from defects, was absent at low temperatures,[40] which indicates that the defect level is below the detection limit.

For chemical identifications of the as-grown samples, X-ray photoelectron spectroscopy (XPS) data of the as-synthesized $MoSe_2$ monolayer on a SiO_2/Si substrate were obtained. The results are indicated in Figure 4. For analysis, the carbon peak binding energy of 284.8 eV was set to a reference to remove any effects of charge accumulation on the samples. The backgrounds were estimated as Shirley-type and fitted from 239.7 to 226.2 eV for Mo and 60.7 to 51.0 eV for Se. Figure 4a shows the characteristic Mo $3d_{5/2}$ and $3d_{3/2}$ peaks from $MoSe_2$ at 229.6 and 232.5 eV respectively, which are almost consistent with the previous reports.[34,35] The peaks from Mo $3d_{5/2}$ and $3d_{3/2}$ of MoO_3 were also identified at 233.1 and 236.2 eV using the data acquired from the MoO_3 film on a SiO_2/Si substrate. The reference peak positions of MoO_3 were reflected to evaluate the presence of residual MoO_3 on the synthesized samples. Figure 4b shows a 3d scan of Se, which indicates that the Se $3d_{5/2}$ and $3d_{3/2}$ peaks from $MoSe_2$ appear at 54.4 and 55.3 eV, respectively,[34,35] and there are no peaks from elemental Se.

Heterostructures of different 2D materials are attracting great interest from the scientific community. The ultrathin nature of each layer can be used to fabricate highly efficient photovoltaics and to solve limitations in scaling down devices. Here, novel heterostructures of $MoSe_2$/graphene were constructed by a series of CVD processes, and their optical properties were investigated using Raman and PL. The results are indicated in Figure 1d. The interesting thing is that while the characteristic peaks of $MoSe_2$ as well as graphene showed up from the series of Raman spectra at 241 cm^{-1} (A_{1g}), 1354 cm^{-1} (D), 1585 cm^{-1} (G), and 2696 cm^{-1} (2D), the $MoSe_2$ peaks at 1.58 eV had almost disappeared or were completely quenched in the PL spectra. The only thing found in the PL was the intrinsic Ar-ion laser (514.5 nm) peak together with a series of peaks from Stokes shifts by graphene *via* inelastic scattering, which exactly match the PL spectra obtained only from graphene. The mechanism is schematically illustrated in Figure 5.

There are two routes for the excitations. First, when electrons from the valence band of $MoSe_2$ are excited by laser light, the electrons are readily transferred to the graphene due to the semimetallic nature of graphene. Here, the charge transfer at the interface between a metal and semiconductors is a commonly observed phenomenon. For example, a recent publication reported that the quenching of PL intensity for monolayer MoS_2 was observed when using gold as a substrate.[39] Since the time scale of nonradiative decay of a charge carrier is much faster than that of recombination between holes and electrons of $MoSe_2$, the intrinsic PL peaks of $MoSe_2$ at 1.58 and 1.76 eV disappear. That is, the following equation is approximately valid.

$$\frac{1}{k_t}+\frac{1}{k_{nd}} \ll \frac{1}{k_r}+\frac{1}{k_{pl}} \qquad (2)$$

where k_t is the rate constant for charge transfer from $MoSe_2$ to graphene, k_{nd} is the rate constant for nonradiative decay in graphene, k_r is the rate constant for relaxation of charge carriers in $MoSe_2$, and k_{pl} corresponds to the rate constant for charge recombination accompanying photoluminescence. Also, from a theoretic viewpoint, the excitonic binding energy and excitonic Bohr radius of the $MoSe_2$ monolayer have been reported as 0.25−0.91 eV[33,35,36] and 0.7 nm,[37] respectively. Considering that the thickness of the monolayer was 0.7 nm[22] (also refer to a step height measurement by AFM in Figure S9), the photogenerated charge carriers could be stably bound until the electron reached the interface with graphene. Then, the immediate charge transfer of electrons to the graphene occurs.

The second way of excitation occurs in graphene. The continuous, Dirac cone-shaped band structure of graphene[1] determines that excitation occurs near the points where the energy difference between the conduction band minimum and valence band maximum corresponds to the energy of external light. During this process, there are always accompanying Stokes and anti-Stokes shifts, although the intensity is relatively small compared to the intrinsic peaks. When an exciton is formed, an electron decays without radiation, which results in no characteristic peaks in the PL.

CONCLUSION

In summary, we demonstrated the growth of a large-area $MoSe_2$ monolayer on dielectric substrates by the CVD method. Raman spectroscopy and PL analysis confirmed that the $MoSe_2$ monolayer was uniformly grown in a large area with high quality and was further characterized by the observation of charged excitons from the low-temperature PL spectrum. In addition, the van der Waals epitaxy of $MoSe_2$ monolayers on graphene has been successfully demonstrated by the same CVD process. The behaviors of photogenerated charge carriers in $MoSe_2$/graphene heterostructures were investigated and were explained by immediate charge transfer to graphene followed by nonradiative recombination. This work is expected to provide a large-area synthesis of transition metal dichalcogenides and van der Waals materials that will engender the development of novel optical and electronic devices.

METHODS

Synthesis of $MoSe_2$ Monolayers. $MoSe_2$ monolayers were prepared by thermal CVD (Figure S1). Molybdenum(VI) oxide (Alfa Aesar, 99.9995%) was dissolved in distilled water; then a drop of solution containing 0.005 g of MoO_3 was placed on a 1 cm × 1 cm piranha-cleaned Si wafer with 300 nm of thermal oxide on it and dried in a vacuum. To trap the precursors and byproducts and for concentrating vapors, a 2 in. quartz tube (90 cm in length) was installed inside the 4 in. quartz tube (120 cm in length). The $MoO_3/SiO_2/Si$ substrate was put on the middle of the chamber and the bare SiO_2/Si substrate was placed next to it. A ceramic boat containing selenium powder (Alfa Aesar, 99.999%, 0.1 g) was positioned slightly upstream (4 cm) of the chamber to maintain its temperature just above the melting point of selenium at reduced pressures. Before starting growth, the chamber was fully evacuated to a pressure below 0.1 mTorr to remove any sources of contamination from air. After flowing 200 sccm of N_2 to maintain the final pressure of 20 Torr, the chamber was heated to 550 °C for 25 min. Ten minutes later, the chamber was heated for 90 min at a ramping rate of 4.4 °C per minute. After 20 min of heating at 950 °C, the heater was turned off and the cover of the furnace was opened to cool the chamber in air for 4 h.

Synthesis of $MoSe_2$/Graphene Heterostructures. Graphene was synthesized by a modified CVD process[38] and transferred onto 300 nm SiO_2/Si substrates by the conventional transfer method.[38] Then the synthesis of $MoSe_2$ monolayers on the substrates was performed by the same CVD process noted for the synthesis of $MoSe_2$ monolayers on SiO_2/Si substrates. For the preparation of TEM samples, graphene was transferred on Mo TEM grids by a PMMA-free transfer method. After that, the synthesis of $MoSe_2$ monolayers on the grids was accomplished using the same CVD process as before.

Mechanical Exfoliation of $MoSe_2$. Mono- and bilayer $MoSe_2$ samples were prepared by mechanical exfoliation of single-crystalline bulk $MoSe_2$ (2D semiconductors) on a Si substrate with 300 nm of thermal oxide on it. The exfoliation was conducted by the conventional Scotch tape method,[21] and the substrate was thoroughly cleaned with piranha solution before sample preparation.

Characterization. Images of the as-grown $MoSe_2$ monolayers were obtained by OM (Leica Reichert Polyvar SC). The synthesized $MoSe_2$ monolayers and $MoSe_2$/graphene heterostructures were analyzed by a micro-Raman and photoluminescence spectrometer (Horiba LabRAM ARAMIS). The excitation source was an Ar-ion laser with its wavelength centered on 514.5 nm, and gratings of 1800 lines/mm and 300 lines/mm were used for Raman and PL measurements, respectively. Before Raman measurements, the peaks were calibrated with the 521.0 cm^{-1} Si peak as a reference. For temperature-dependent PL spectra, the samples were placed on a Linkam THMS600 stage, and then the temperature was adjusted by regulating both the flow rate of liquid N_2 passing through the stage and the heating rate of the stage using an LNP95 cooling system and T95 LinkPad controller. Compositional data were obtained by XPS (Thermo VG Scientific Sigma

Probe spectrometer) using a monochromatic Al Kα (1486.6 eV) source. The alignments between the monolayer $MoSe_2$ and the graphene support were analyzed by Cs-corrected STEM (JEM-ARM200F).

Conflict of Interest: The authors declare no competing financial interest.

Acknowledgment. This work was supported by grants from Global Frontier Research Center for Advanced Soft Electronics (2011-0031640), Nano-Material Technology Development Program of NRF (2012M3A7B4049807), and LG Display Co., Ltd.

Supporting Information Available: Reaction schemes of CVD; strategies on the precursor selection; safety measures for the experiment; STEM image of $MoSe_2$/graphene on a Mo grid; reference Raman/PL spectra of source materials, substrates, and exfoliated mono- and bilayer $MoSe_2$ samples; plot of PL intensities with temperatures; photograph of CVD-grown large-area $MoSe_2$; optical, Raman/PL intensity/position mapping, AFM images of samples; schematics of CVD growth. This material is available free of charge *via* the Internet at http://pubs.acs.org.

REFERENCES AND NOTES

1. Zhou, S. Y.; Gweon, G. H.; Graf, J.; Fedorov, A. V.; Spataru, C. D.; Diehl, R. D.; Kopelevich, Y.; Lee, D. H.; Louie, S. G.; Lanzara, A. First Direct Observation of Dirac Fermions in Graphite. *Nat. Phys.* **2006**, *2*, 595–599.
2. Splendiani, A.; Sun, L.; Zhang, Y.; Li, T.; Kim, J.; Chim, C.-Y.; Galli, G.; Wang, F. Emerging Photoluminescence in Monolayer MoS_2. *Nano Lett.* **2010**, *10*, 1271–1275.
3. Zhao, W.; Ghorannevis, Z.; Chu, L.; Toh, M.; Kloc, C.; Tan, P.-H.; Eda, G. Evolution of Electronic Structure in Atomically Thin Sheets of WS_2 and WSe_2. *ACS Nano* **2012**, *7*, 791–797.
4. Tongay, S.; Zhou, J.; Ataca, C.; Lo, K.; Matthews, T. S.; Li, J.; Grossman, J. C.; Wu, J. Thermally Driven Crossover from Indirect toward Direct Bandgap in 2D Semiconductors: $MoSe_2$ *versus* MoS_2. *Nano Lett.* **2012**, *12*, 5576–5580.
5. Mak, K. F.; Lee, C.; Hone, J.; Shan, J.; Heinz, T. F. Atomically Thin MoS_2: A New Direct-Gap Semiconductor. *Phys. Rev. Lett.* **2010**, *105*, 136805.
6. Bernardi, M.; Palummo, M.; Grossman, J. C. Semiconducting Monolayer Materials as a Tunable Platform for Excitonic Solar Cells. *ACS Nano* **2012**, *6*, 10082–10089.
7. Bernardi, M.; Palummo, M.; Grossman, J. C. Extraordinary Sunlight Absorption and One Nanometer Thick Photovoltaics Using Two-Dimensional Monolayer Materials. *Nano Lett.* **2013**, *13*, 3664–3670.
8. Buscema, M.; Barkelid, M.; Zwiller, V.; van der Zant, H. S. J.; Steele, G. A.; Castellanos-Gomez, A. Large and Tunable Photothermoelectric Effect in Single-Layer MoS_2. *Nano Lett.* **2013**, *13*, 358–363.
9. Voiry, D.; Yamaguchi, H.; Li, J.; Silva, R.; Alves, D. C. B.; Fujita, T.; Chen, M.; Asefa, T.; Shenoy, V. B.; Eda, G.; *et al.* Enhanced Catalytic Activity in Strained Chemically Exfoliated WS_2 Nanosheets for Hydrogen Evolution. *Nat. Mater.* **2013**, *12*, 850–855.
10. Mak, K. F.; He, K.; Shan, J.; Heinz, T. F. Control of Valley Polarization in Monolayer MoS_2 by Optical Helicity. *Nat. Nanotechnol.* **2012**, *7*, 494–498.
11. Radisavljevic, B.; Radenovic, A.; Brivio, J.; Giacometti, V.; Kis, A. Single-Layer MoS_2 Transistors. *Nat. Nanotechnol.* **2011**, *6*, 147–150.
12. Eda, G.; Yamaguchi, H.; Voiry, D.; Fujita, T.; Chen, M.; Chhowalla, M. Photoluminescence from Chemically Exfoliated MoS_2. *Nano Lett.* **2011**, *11*, 5111–5116.
13. Zeng, Z.; Yin, Z.; Huang, X.; Li, H.; He, Q.; Lu, G.; Boey, F.; Zhang, H. Single-Layer Semiconducting Nanosheets: High-Yield Preparation and Device Fabrication. *Angew. Chem., Int. Ed.* **2011**, *50*, 11093–11097.
14. Coleman, J. N.; Lotya, M.; O'Neill, A.; Bergin, S. D.; King, P. J.; Khan, U.; Young, K.; Gaucher, A.; De, S.; Smith, R. J.; *et al.* Two-Dimensional Nanosheets Produced by Liquid Exfoliation of Layered Materials. *Science* **2011**, *331*, 568–571.
15. Gutiérrez, H. R.; Perea-López, N.; Elías, A. L.; Berkdemir, A.; Wang, B.; Lv, R.; López-Urías, F.; Crespi, V. H.; Terrones, H.; Terrones, M. Extraordinary Room-Temperature Photoluminescence in Triangular WS_2 Monolayers. *Nano Lett.* **2012**, *13*, 3447–3454.
16. Huang, J.-K.; Pu, J.; Hsu, C.-L.; Chiu, M.-H.; Juang, Z.-Y.; Chang, Y.-H.; Chang, W.-H.; Iwasa, Y.; Takenobu, T.; Li, L.-J. Large-Area Synthesis of Highly Crystalline WSe_2 Monolayers and Device Applications. *ACS Nano* **2013**, *8*, 923–930.
17. Lee, Y.-H.; Zhang, X.-Q.; Zhang, W.; Chang, M.-T.; Lin, C.-T.; Chang, K.-D.; Yu, Y.-C.; Wang, J. T.-W.; Chang, C.-S.; Li, L.-J.; *et al.* Synthesis of Large-Area MoS_2 Atomic Layers with Chemical Vapor Deposition. *Adv. Mater.* **2012**, *24*, 2320–2325.
18. Zhan, Y.; Liu, Z.; Najmaei, S.; Ajayan, P. M.; Lou, J. Large-Area Vapor-Phase Growth and Characterization of MoS_2 Atomic Layers on a SiO_2 Substrate. *Small* **2012**, *8*, 966–971.
19. Zhu, Z. Y.; Cheng, Y. C.; Schwingenschlögl, U. Giant Spin-Orbit-Induced Spin Splitting in Two-Dimensional Transition-Metal Dichalcogenide Semiconductors. *Phys. Rev. B* **2011**, *84*, 153402.
20. Hwang, J.; Kim, M.; Campbell, D.; Alsalman, H. A.; Kwak, J. Y.; Shivaraman, S.; Woll, A. R.; Singh, A. K.; Hennig, R. G.; Gorantla, S.; *et al.* Van der Waals Epitaxial Growth of Graphene on Sapphire by Chemical Vapor Deposition without a Metal Catalyst. *ACS Nano* **2012**, *7*, 385–395.
21. Tonndorf, P.; Schmidt, R.; Böttger, P.; Zhang, X.; Börner, J.; Liebig, A.; Albrecht, M.; Kloc, C.; Gordan, O.; Zahn, D. R. T. Photoluminescence Emission and Raman Response of Monolayer MoS_2, $MoSe_2$, and WSe_2. *Opt. Express* **2013**, *21*, 4908–4916.
22. Ross, J. S.; Wu, S.; Yu, H.; Ghimire, N. J.; Jones, A. M.; Aivazian, G.; Yan, J.; Mandrus, D. G.; Xiao, D.; Yao, W.; *et al.* Electrical Control of Neutral and Charged Excitons in a Monolayer Semiconductor. *Nat. Commun.* **2013**, *4*, 1474.
23. Beal, A. R.; Hughes, H. P. Kramers-Kronig Analysis of the Reflectivity Spectra of 2H-MoS_2, 2H-$MoSe_2$ and 2H-$MoTe_2$. *J. Phys. C: Solid State Phys.* **1979**, *12*, 881.
24. Liu, G.-B.; Shan, W.-Y.; Yao, Y.; Yao, W.; Xiao, D. Three-Band Tight-Binding Model for Monolayers of Group-VIB Transition Metal Dichalcogenides. *Phys. Rev. B* **2013**, *88*, 085433.
25. Zhang, Y.; Zhang, Y.; Ji, Q.; Ju, J.; Yuan, H.; Shi, J.; Gao, T.; Ma, D.; Liu, M.; Chen, Y.; *et al.* Controlled Growth of High-Quality Monolayer WS_2 Layers on Sapphire and Imaging Its Grain Boundary. *ACS Nano* **2013**, *7*, 8963–8971.
26. Mann, J.; Sun, D.; Ma, Q.; Chen, J.-R.; Preciado, E.; Ohta, T.; Diaconescu, B.; Yamaguchi, K.; Tran, T.; Wurch, M.; *et al.* Facile Growth of Monolayer MoS_2 Film Areas on SiO_2. *Eur. Phys. J. B* **2013**, *86*, 1–4.
27. Zhao, W.; Ribeiro, R. M.; Toh, M.; Carvalho, A.; Kloc, C.; Castro Neto, A. H.; Eda, G. Origin of Indirect Optical Transitions in Few-Layer MoS_2, WS_2 and WSe_2. *Nano Lett.* **2013**, *13*, 5627–5634.
28. Zeghbroeck, B. *Principles of Semiconductor Devices and Heterojunctions*, 1st ed.; Prentice Hall PTR: New Jersey, 2008.
29. Varshni, Y. P. Temperature Dependence of the Energy Gap in Semiconductors. *Physica* **1967**, *34*, 149–154.
30. Kang, J.; Tongay, S.; Zhou, J.; Li, J.; Wu, J. Band Offsets and Heterostructures of Two-Dimensional Semiconductors. *Appl. Phys. Lett.* **2013**, *102*, 012111–4.
31. Larentis, S.; Fallahazad, B.; Tutuc, E. Field-Effect Transistors and Intrinsic Mobility in Ultra-Thin $MoSe_2$ Layers. *Appl. Phys. Lett.* **2012**, *101*, 223104–4.
32. Mak, K. F.; He, K.; Lee, C.; Lee, G. H.; Hone, J.; Heinz, T. F.; Shan, J. Tightly Bound Trions in Monolayer MoS_2. *Nat. Mater.* **2013**, *12*, 207–211.
33. Berkelbach, T. C.; Hybertsen, M. S.; Reichman, D. R. Theory of Neutral and Charged Excitons in Monolayer Transition Metal Dichalcogenides. *Phys. Rev. B* **2013**, *88*, 045318.
34. Abdallah, W. e.; Nelson, A. E. Characterization of $MoSe_2$-(0001) and Ion-Sputtered $MoSe_2$ by XPS. *J. Mater. Sci.* **2005**, *40*, 2679–2681.

35. Hao, T.; Dou, K.; Kaun, C.-C.; Kuang, Q.; Yang, S. $MoSe_2$ Nanosheets and Their Graphene Hybrids: Synthesis, Characterizations and Hydrogen Evolution Reaction Studies. *J. Mater. Chem. A* **2014**, *2*, 360–364.
36. Komsa, H.-P.; Krasheninnikov, A. V. Effects of Confinement and Environment on the Electronic Structure and Exciton Binding Energy of MoS_2 from First Principles. *Phys. Rev. B* **2012**, *86*, 241201.
37. Ross, J. S.; Wu, S.; Yu, H.; Ghimire, N. J.; Jones, A. M.; Aivazian, G.; Yan, J.; Mandrus, D. G.; Xiao, D.; Yao, W.; *et al*. Electrical Control of Two-Dimensional Neutral and Charged Excitons in a Monolayer Semiconductor. *arXiv:1211.0072*, **2012**.
38. Li, X.; Zhu, Y.; Cai, W.; Borysiak, M.; Han, B.; Chen, D.; Piner, R. D.; Colombo, L.; Ruoff, R. S. Transfer of Large-Area Graphene Films for High-Performance Transparent Conductive Electrodes. *Nano Lett.* **2009**, *9*, 4359–4363.
39. Bhanu, U.; Islam, M. R.; Tetard, L.; Khondaker, S. I., Photoluminescence quenching in gold - MoS_2 hybrid nanoflakes. *Sci. Rep.* **2014**, *4*, 5575.
40. Tongay, S.; Suh, J.; Ataca, C.; Fan, W.; Luce, A.; Kang, J. S.; Liu, J.; Ko, C.; Raghunathanan, R.; Zhou, J.; *et al*. Defects activated photoluminescence in two-dimensional semiconductors: interplay between bound, charged, and free excitons. *Sci. Rep.* **2013**, *3*, 2657.